

Monte Carlo based performance assessment of different animal PET architectures using pixellated CZT detectors

D. Visvikis^{a,*}, T. Lefevre^a, F. Lamare^a, G. Kontaxakis^b, A. Santos^b, D. Darambara^c

^aINSERM U650, LaTIM, University Hospital Medical School, F-29609 Brest, France

^bETSI Telecomunicacion Universidad Politecnica de Madrid, Ciudad Universitaria, s/n 28040, Madrid, Spain

^cDepartment of Physics, School of Engineering and Physical Sciences, University of Surrey, Guildford, UK

Available online 11 September 2006

Abstract

The majority of present position emission tomography (PET) animal systems are based on the coupling of high-density scintillators and light detectors. A disadvantage of these detector configurations is the compromise between image resolution, sensitivity and energy resolution. In addition, current combined imaging devices are based on simply placing back-to-back and in axial alignment different apparatus without any significant level of software or hardware integration. The use of semiconductor CdZnTe (CZT) detectors is a promising alternative to scintillators for gamma-ray imaging systems. At the same time CZT detectors have the potential properties necessary for the construction of a truly integrated imaging device (PET/SPECT/CT). The aims of this study was to assess the performance of different small animal PET scanner architectures based on CZT pixellated detectors and compare their performance with that of state of the art existing PET animal scanners. Different scanner architectures were modelled using GATE (Geant4 Application for Tomographic Emission). Particular scanner design characteristics included an overall cylindrical scanner format of 8 and 24 cm in axial and transaxial field of view, respectively, and a temporal coincidence window of 8 ns. Different individual detector modules were investigated, considering pixel pitch down to 0.625 mm and detector thickness from 1 to 5 mm. Modified NEMA NU2-2001 protocols were used in order to simulate performance based on mouse, rat and monkey imaging conditions. These protocols allowed us to directly compare the performance of the proposed geometries with the latest generation of current small animal systems. Results attained demonstrate the potential for higher NECR with CZT based scanners in comparison to scintillator based animal systems.

© 2006 Elsevier B.V. All rights reserved.

PACS: 05.10.Ln; 28.41.Rc; 42.79.Pw; 61.82.Fk

Keywords: Monte Carlo; GATE; Dosimetry; Efficiency

1. Introduction

Present commercially available positron emission tomography (PET) and single photon emission tomography (SPET) clinical and small animal imaging devices are based on the coupling of high-density scintillation detectors with photomultiplier tubes (PMTs). The disadvantage of this approach is the compromise between the potential image resolution which implies an as small as possible crystal surface area and on the other hand as long as possible crystal elements to facilitate high sensitivity and energy resolution. Unfortunately, these two requirements are

incompatible defining the absolute limits of spatial resolution in in-vivo molecular imaging with such traditional detectors of the range of 1 mm, without considering limitations in sensitivity and energy resolution associated with achieving such a spatial resolution. In addition, such a detector configuration excludes any capability of performing meaningful X-ray CT imaging.

Consequently current combined imaging devices, in the clinical as well as animal imaging environment, are based on simply placing coaxially the different apparatus without any significant level of integration in either hardware or software. Effectively the only real element of integration with present systems is the use of the same examination bed for all imaging devices. This lack of integration does not facilitate simultaneous imaging in either space or time,

*Corresponding author. Tel.: +33 29 8018114; fax: +33 29 8018124.

E-mail address: Visvikis.Dimitris@univ-brest.fr (D. Visvikis).

leading to a number of associated compromises as far as the goals of molecular imaging are concerned. Since the images are effectively acquired at different times with two different scanners, they cannot be perfectly co-registered due to subject movement between scans, or more generally, due to normal physiological processes, such as respiratory motion or bowel progression through the gastro-intestinal tract. These problems are amplified when high resolution imaging is necessary. Furthermore, it is not possible to follow complementary biochemical processes and their changes as a function of time constituting a major limitation considering the needs imposed by the potential applications of molecular imaging. Finally, the lack of true integration does not lead to an associated reduction in the cost of such combined imaging devices which is similar to a corresponding multiple of the individual systems' costs.

As an alternative, wide gap semiconductor detector materials, exhibit the necessary basic properties for the construction of high resolution emission tomography systems without an associated compromise in system sensitivity. In recent years, considerable improvements have been made with CdZnTe (CZT) detector spectral properties based on the advances in the production of crystals (high-pressure Bridgman growth technique) and the design of electrodes [1]. Single polarity charge sensing through a coplanar grid electrode, has been widely applied to CZT detectors to overcome poor hole-transport. In a coplanar grid detector the induced signal on the cathode increases approximately linearly with interaction distance from the anodes, whereas the signal on each coplanar anode is mainly depth independent. However, even with single polarity charge sensing techniques and methods to compensate for electron trapping, such as relative gain and depth sensing, the variations in electron trapping and material non-uniformity can still degrade the energy resolution. The effects of hole-trapping can be significantly reduced in CZT multi-element pixel array detectors due to the “small pixel effect”, which can have a dramatic impact on the pulse-height spectrum with many more of the events concentrated in the photopeak.

In addition, these detector materials can efficiently detect X-rays [2], as well as been able to operate in the presence of a magnetic field. These combined properties make CZT multi-element pixel array detectors a potential candidate for the construction of a truly integrated imaging device, allowing SPET/PET/CT imaging to be realized inside the magnetic field of an MRI scanner. In order to realize such a combined system a number of developments will be necessary in detector and electronics technology as well as in system architecture design.

The sensitivity of CZT multi-element pixel array detectors is sufficient for SPET imaging, considering the thickness that can be achieved with sufficiently high material uniformity. However, in the case of high energy photons involved in PET imaging, different system architectures have to be considered in order to attain the necessary material thickness for high detection sensitivity,

without at the same time compromising the high spatial resolution offered by such pixellated detectors. The objectives of this work were to (i) assess the performance of different CZT pixellated detector arrangements in comparison to the performance of state of the art existing PET animal scanners, and (ii) optimise individual detector panel characteristics leading to optimum overall performance for each of the PET scanner detector arrangements considered. A cylindrical detector arrangement was imposed in the design considerations since despite the present study concerning the PET component imaging performance assessment, the final objective is the construction of an integrated PET/SPET/CT system.

2. Materials and methods

2.1. Monte Carlo simulations

GATE was used to perform an accurate simulation of the different detector configurations considered [3]. GATE was chosen since it allows easy description of complicated emission tomography system designs and associated signal flows in order to specify the electronics performance requirements necessary for each detector configuration considered.

In order to validate the simulations, measurements were carried out using a single pixellated CZT module. The module consists of an eV Products detector coupled to a low-noise, low-power multi-channel XA1.6 readout ASIC from IDEAS, which uses a self-generated asynchronous trigger with pixel-level addressing. The CZT detector consists of 16×16 pixels with a 2.46 mm pixel pitch ($40 \text{ mm} \times 40 \text{ mm}$ overall surface area) and a 5 mm thickness. An energy resolution at single pixel level of 2.8% and 4.3% FWHM at 140 and 662 keV, respectively, was measured using $^{99\text{m}}\text{Tc}$ and ^{137}Cs point sources.

2.2. Detector modules and overall scanner geometries

An overall cylindrical scanner format of 8 cm in axial field of view and a transaxial field of view of 26 cm were considered. The overall dimensions of the individual pixellated detector panels used were fixed to 40 mm by 40 mm, while the pixel pitch and detector thickness were allowed to vary from 0.625 to 2.5 mm and from 1 to 5 mm, respectively. A coincidence temporal window of 8 ns, and an energy window of 300–650 keV was used.

Two different detector module arrangements were investigated using GATE. The first geometry called “planar” (see Fig. 1), assumes that the $40 \text{ mm} \times 40 \text{ mm}$ panels are facing towards the inside of the imaging field of view. Each detection module is made of multiple pixellated panels placed one on the top of the other. A total module thickness of 40 mm (for example $8 \times 5 \text{ mm}$ thick panels) was considered. On the second geometry called “linear” (see Fig. 2), the individual panels are placed vertically with the smaller dimension of each pixellated panel

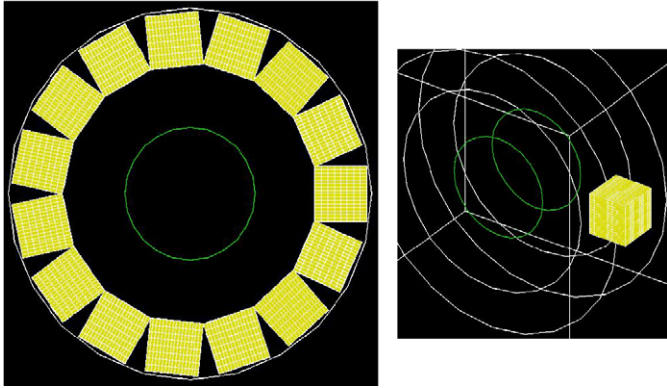


Fig. 1. The “planar” design. The insert on the right hand side shows one of the modules.

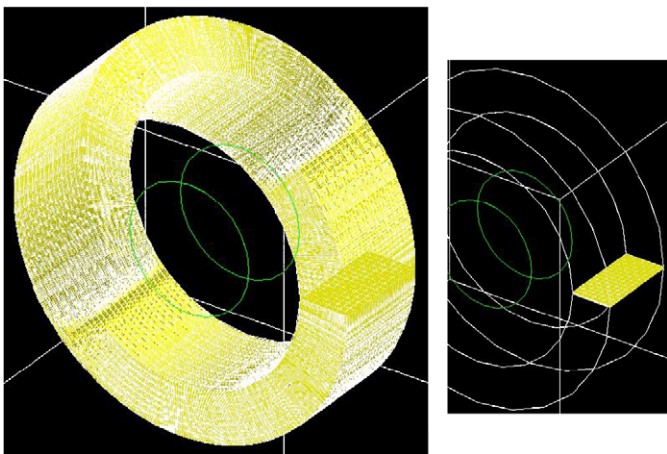


Fig. 2. The “linear” design with the modules placed vertically (the thickness dimension of each module facing towards the inside of the imaging field of view). The insert on the right hand side shows one of the modules.

(corresponding to its thickness) facing towards the inside of the imaging field of view.

No modeling of electronics and associated signal flow were considered.

2.3. Count rate performance assessment

Similar protocols to these used during the performance assessment of the microPET Focus scanner [4], were employed in order to allow a direct comparison. The microPET Focus is a state of the art commercially available small animal PET scanner based on the use of LSO crystals coupled to position sensitive PMTs using optical fiber bundles. The count rate performance was assessed using the NEMA NU2-2001 protocol [5]. Different diameter solid polyethylene cylinders were used simulating mouse and rat imaging conditions. The diameters used were 3, 6 and 10 cm, with a length of 7, 15 and 40 cm considering mouse, rat and monkey imaging conditions, respectively (Fig. 3). A line source as long as the axial extent of each phantom was placed off centre.

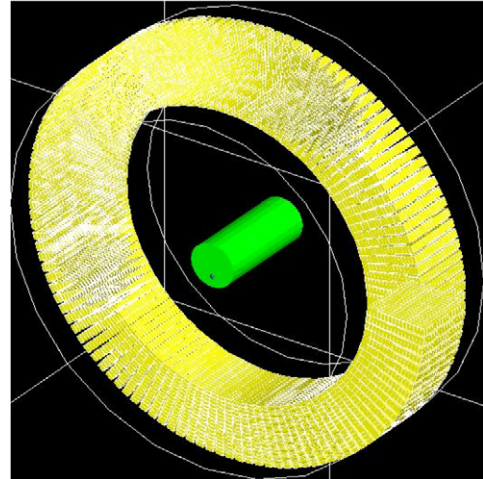


Fig. 3. The mouse phantom used in the count rate performance evaluation, showing the position of the long line source, and the phantom placement in the scanner's field of view.

Progressively larger amounts of activity were simulated in the line source in order to recover the count rate behaviour of the system as a function of activity present in the phantom. Since no electronics dead time or associated signal flow effects were modeled, the activity levels for each of the phantoms considered were kept within the range where minimum dead time effects were demonstrated for the microPET Focus. Using the simulated count rates the scatter fraction was calculated. In addition, the noise equivalent count rates (NECR) [6] as a function of activity were calculated from the simulated count rates and compared to measurements using the following expression

$$\text{NECR} = \frac{T^2}{T + S + 2aR} \quad (1)$$

where, T , S and R are the number of trues, scattered and random coincidences, respectively, and a is the fraction of the object in the field of view.

3. Results

The simulated energy resolution for the single multi-element pixellated CZT detector panel was close to the measured at 3.0% and 4.6% for the $^{99\text{m}}\text{Tc}$ and ^{137}Cs point sources, respectively.

Figs. 4 and 5 show the NECR vs activity concentration in the mouse phantom for the different detector panel configurations considered in the “planar” and “linear” architecture designs, respectively. A similar dependency to the NEMA NU2-2001 mouse phantom results as far as the individual module parameters are concerned was also observed under rat imaging conditions. A global reduction in the NECR of a factor of 10 was seen using the NEMA NU2-2001 rat phantom in comparison to the mouse phantom results.

Figs. 6 and 7 show the NECR vs activity concentration in the mouse and rat phantoms for the different CZT

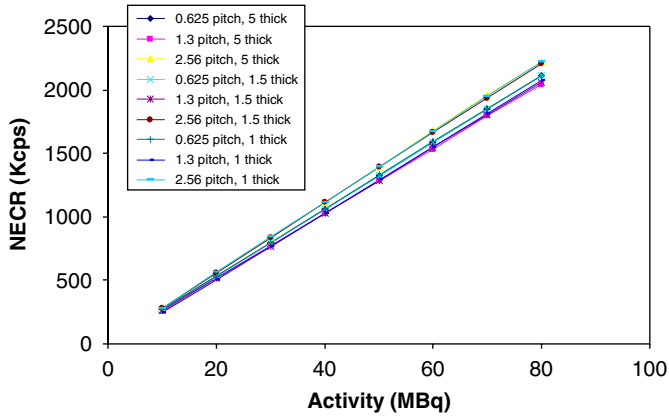


Fig. 4. NECR vs activity concentration in the mouse phantom for the “planar” PET scanner architecture.

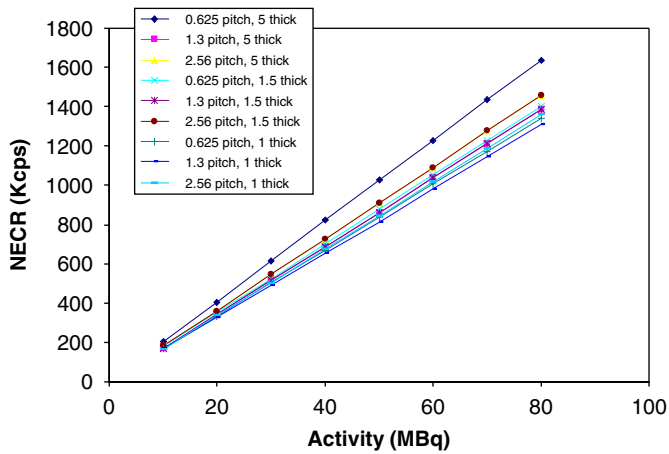


Fig. 5. NECR vs activity concentration in the mouse phantom for the “linear” PET scanner architecture.

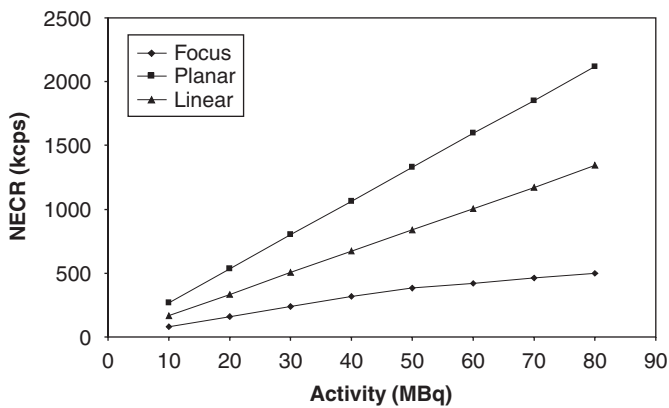


Fig. 6. NECR vs activity concentration using the mouse phantom for the two CZT architectures (individual module parameters: 0.625 mm pitch, 1 mm thick) and the LSO based microPET Focus [4].

scanner architectures considered and the microPET Focus. The individual module dimension used to obtain the data in Figs. 6 and 7 were 0.625 mm pitch size and 1 mm in thickness.

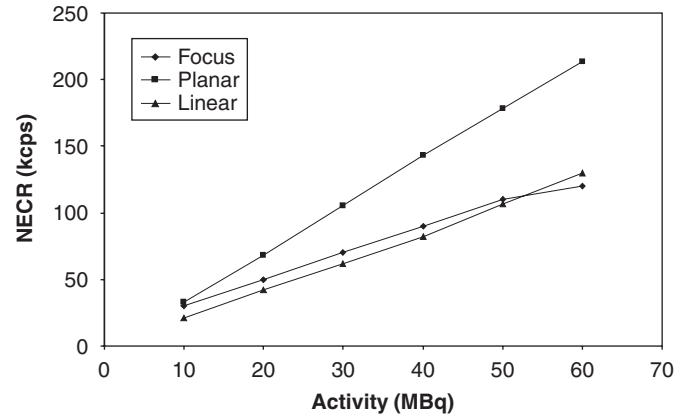


Fig. 7. NECR vs activity concentration using the rat phantom for the two CZT architectures (individual module parameters: 0.625 mm pitch, 1 mm thick) and the LSO based microPET Focus [4].

A scatter fraction of 12% and 14.5% was recorded in the rat phantom considering the “linear” and the “planar” CZT scanner architectures. This relative difference in the scatter fraction between the two scanner designs was constant irrespective of the phantom size considered.

Finally, in terms of random coincidences a larger fraction by 33% and 15% were registered in the case of the “planar” design relative to the “linear” design under rat and mouse imaging conditions, respectively.

4. Discussion and conclusions

Semiconductor detectors have properties that could allow the improvement of current spatial resolution in emission tomography without any compromise in overall sensitivity. Furthermore, such detectors may allow the true integration of different imaging modalities using a single detector material.

We have evaluated, in terms of PET NECR performance under various imaging conditions, two different scanner architectures based on multi-element pixellated CZT detector modules. Such detector modules possess inherent depth of interaction information at the level of individual pixels, the size of which will ultimately determine the level of spatial resolution that can be achieved.

Despite performing worse in terms of scatter and random coincidences, the “planar” design leads to an overall higher NECR vs activity concentration for the different imaging conditions evaluated in comparison to the “linear” design. This was also the case considering a comparison with the NECR performance of current state of the art scintillator based animal scanners. Although a thin CZT module implemented in the “linear” scanner design will allow a uniform resolution to be realized the size of the “dead space” necessary between individual detector modules leads to a significantly reduced count rate performance in comparison to the “planar” design and similar to that of the microPET Focus.

In conclusion, the “planar” scanner design using a pixel size of 0.625 mm and an individual module thickness of 1 mm should lead to improved spatial resolution and a greater than a factor of 3 improvement in the NECR performance relative to current scintillator based PET scanners under different imaging conditions.

References

- [1] T. Takahashi, S. Watanabe, IEEE Trans. Nucl. Sci. NS-48 (4) (2001) 950.
- [2] S.R. Cherry, J.A. Sorenson, M.E. Phelps, Physics in Nuclear Medicine, third ed, Saunders—Elsevier Science Eds., USA, 2003.
- [3] S. Jan, G. Santin, D. Strul, et al., Phys. Med. Biol. 49 (2004) 4543.
- [4] Y.C. Tai, A. Ruangma, D. Rowland, et al., J. Nucl. Med. 46 (2005) 455.
- [5] Performance Measurements of Positron Emission Tomographs, National Electrical Manufacturers Association, NEMA Standards Publication NU2-2001, Washington DC, 2001.
- [6] S.C. Strother, E. Hoffman, et al., IEEE Trans. Nucl. Sci. NS-37 (1990) 783.